Supporting Information

Ferromagnetic Transformation of α-Fe_2O_3 via Co Doping for Efficient Water Oxidation under Magnetic Field

Hong Wang,[a†] Yuan Dong,[a†] Jie Ying,*[b†] Ziheng Zhu,[a] Yuan Feng,[a] Yuxuan Xiao,[b] Ge Tian,[a] Ling Shen,[a] Wei Geng,[b] Yi Lu,[ac] Siming Wu,[a] Xiaoyu Yang*[ac]

[a.] *State Key Laboratory of Silicate Materials for Architectures & State Key Laboratory of Advanced Technology for Materials Synthesis and Processing & School of Chemistry, Chemical Engineering and Life Sciences & Laoshan Laboratory & School of Materials Science and Engineering & International School of Materials Science and Engineering, Wuhan University of Technology, Wuhan, 430070, China.*

[b.] *School of Chemical Engineering and Technology, Sun Yat-sen University, Zhuhai, 519082, China.*

[c.] *National energy key laboratory for new hydrogen-ammonia energy technologies, Foshan Xianhu Laboratory, Foshan 528200, P. R. China.*

[†] *Both authors contributed equally to the work.*

*Corresponding Author

Email: xyyang@whut.edu.cn; yingj5@mail.sysu.edu.cn

METHODS

Chemical and Materials: All reagents were commercially available and used as received without further purification. The water used throughout all experiments was Milli–Q Millipore deionized water.

Preparation of α-Fe_2O_3: The required amount of $FeCl_3 \cdot 6H_2O$ (20 mmol) was dissolved in 100 ml of deionized water, and precipitation was induced using 15 mmol of NaOH. The reaction solution was heated in a water bath at 85 °C for 1 hour. After cooling, the solution was subjected to centrifugation, and the resulting material was dried overnight at 110 °C. After grinding, the material was heat-treated in a muffle furnace at 550 °C for 2 hours, followed by further heating at 1000 °C for 1 hour (with a heating rate of 5 °C min^{-1}). Finally, black powdered α-Fe_2O_3 was synthesized.

Preparation of cobalt-doped α-Fe_2O_3: The required amounts of $CoCl_2 \cdot 6H_2O$ (10, 40, 160 or 240 mmol) and $FeCl_3 \cdot 6H_2O$ (20 mmol) were dissolved in 100 ml of deionized water, and precipitation was induced using 15 mmol of NaOH. The reaction solution was heated in a water bath at 85 °C for 1 hour. After cooling, the solution was subjected to centrifugation, and the resulting material was dried overnight at 110 °C. After grinding, the material was heat-treated in a muffle furnace at 550 °C for 2 hours, followed by further heating at 1000 °C for 1 hour (with a heating rate of 5 °C min^{-1}). Finally, black powdered cobalt-doped α-Fe_2O_3 was synthesized.

Carbon cloth substrate pretreatment: First, the carbon cloth (size: 1×1.5 cm^2, CC) was soaked in a concentrated sulfuric acid and nitric acid mixture (volume ratio 3:1) for 12 hours, then rinsed three times with deionized water. Next, deionized water was added, and the cloth was sonicated for 20 minutes to thoroughly remove the sulfuric and nitric acids from the carbon cloth. Finally, it was dried in a vacuum drying oven at 60 °C.

Preparation of electrode: First, 10 mg of catalyst powder was added to a mixture of 950 μL isopropanol and 50 μL of 5 wt.% Nafion solution, followed by sonication to evenly disperse the catalyst in the mixture. Then, 100 μL of the mixture was drawn using a pipette and applied evenly in multiple steps onto the surface of a 1 cm^2 carbon cloth. The electrode was allowed to air dry naturally.

Physical characterization: XRD analysis was tested via a Bruker D8 Advance X-ray diffractometer (Bruker) equipped with Cu Kα radiation (λ = 1.540598 Å). The SEM (HITACHI S-4800) and TEM (JEOL JEM-2100F) were used to characterize the morphology and structure of the catalysts. XPS was applied to analyze the chemical composition. The Vibrating Sample Magnetometer (VSM) was used to measure the magnetic characteristics of materials, such as magnetization, hysteresis loops, coercivity, saturation magnetization, and remanence. The elemental composition and content of the material were measured by inductively coupled plasma atomic emission spectrometry (ICP-AES, Prodigy 7, LEEMAN LABS INC, USA).

Electrochemical characterization: All electrochemical tests were performed at room temperature using an Autolab PG 302N electrochemical analyzer with a three-electrode system injected with 1 M KOH water. The reference electrode was a standard Ag/AgCl (saturated) electrode, and the counter electrode was a graphite bar. All potentials measured were calibrated to RHE using the following equation:

$$E_{RHE} = E_{Ag/AgCl} + 0.0592 \times pH + E^0_{Ag/AgCl} \quad \text{(S1)}$$

where E_{RHE} is the converted potential vs. RHE, $E^0_{Ag/AgCl} = 0.196$ at 25 °C, and $E_{Ag/AgCl}$ is the experimentally measured potential against the Ag/AgCl reference. The current density was normalized to the geometric area of the electrode. Linear sweep voltammetry (LSV) curves were recorded at a scan rate of 2 mV s^{-1} after the catalysts had undergone approximately 50 cycles at a scan rate of 100 mV s^{-1} between 1.2 and 1.53 V versus a reversible hydrogen electrode (RHE), until a stable cyclic voltammetry (CV) curve was obtained. The double-layer capacitance (C_{dl}) was determined by conducting cyclic voltammetry (CV) measurements at various sweep rates within a specific voltage range of the non-Faradaic region. By linearly fitting the current response to the sweep rate, the electrochemical active area of the catalyst could be inferred. The electrochemically active surface area (ECSA) was evaluated by C_{dl} with CVs at different scan rates of 20-100 mV s^{-1}. According to the formula ECSA = C_{dl} / C_s, C_s = 40 μF cm^{-2}, the value of ECSA is positively correlated with C_{dl}.[1] The CV sweep rate range employed was 1.15-1.25 V (vs RHE). The electronic transfer resistance at the catalyst/electrolyte interface during the catalytic process was evaluated using electrochemical impedance spectroscopy (EIS) measurements. The percentage change in charge transfer resistanceis (ΔR_{ct} (%)) is computed using the following equation:

$$\Delta R_{ct}\,(\%) = (R_{ct,\ Without\ H} - R_{ct,\ With\ H}) / R_{ct,\ Without\ H} \times 100\% \quad (S2)$$

where $R_{ct,\ Without\ H}$ and $R_{ct,\ With\ H}$ represent the charge transfer resistance under the absence and presence of a magnetic field, respectively. The magnetic current is computed using the following equation:

$$\text{magnetic current}\ (\%) = (J(M_{ON}) - J(M_{OFF})) / J(M_{OFF}) \times 100\% \quad (S3)$$

where J represents the current density. iR-compensation was applied to all polarization curves based on resistance data. Durability tests for the electrocatalyst/electrode were conducted by applying chronoamperometric curves at a fixed current density. All error bars in this paper represent the standard deviation obtained from three independent measurements.

Supplementary Experiment Sections

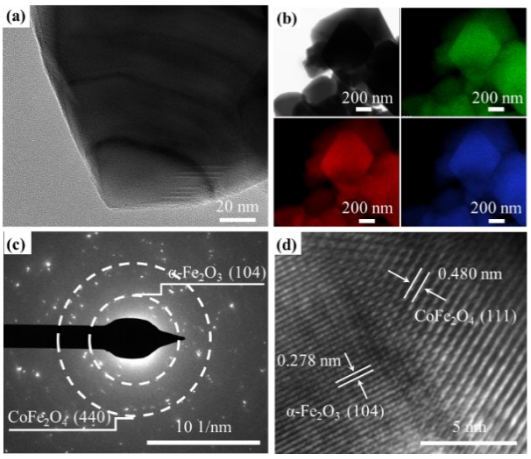

Figure S1. (a) Low magnification TEM image of $Co_{0.14}FeO_x$. (b) TEM image with corresponding element mapping of $Co_{0.14}FeO_x$. (c) The selected area electron diffraction pattern of $Co_{0.14}FeO_x$. (d) A HRTEM image of $Co_{0.14}FeO_x$.

Note: $Co_{0.14}FeO_x$ exhibits a complete spinel structure with a uniform distribution of elements. Additionally, the selected area electron diffraction (SAED) detected diffraction patterns corresponding to both α-Fe_2O_3 and $CoFe_2O_4$ phases. Further, the HRTEM image of $Co_{0.14}FeO_x$ clearly shows the lattice fringes of both α-Fe_2O_3 and $CoFe_2O_4$ phases which are in close contact at the interface. The above experimental results suggest that α-Fe_2O_3 and $CoFe_2O_4$ are likely to form a heterojunction through interface contact at the microscopic scale instead of existing in a solid solution or mixed state.

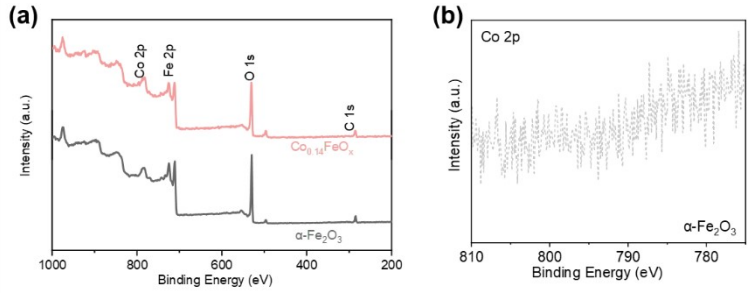

Figure S2. (a) XPS full spectrum of α-Fe_2O_3 and $Co_{0.14}FeO_x$. (b) The Co 2p XPS spectra result of α-Fe_2O_3 sample.

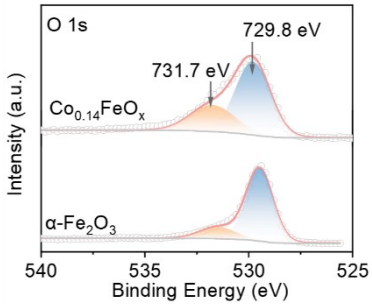

Figure S3. The O 1s XPS spectra result of α-Fe_2O_3 and $Co_{0.14}FeO_x$ samples.

Note: The peak of O 1s with the binding energy of 731.7 eV is ascribed to sorbed water (H_2O).

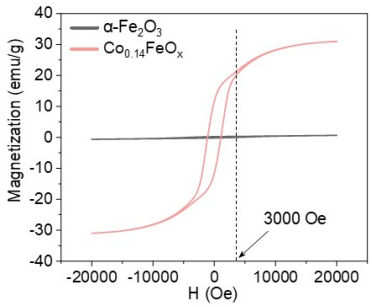

Figure S4. The magnetization corresponding to α-Fe_2O_3 and $Co_{0.14}FeO_x$ under an external magnetic field strength of 3000 Oe.

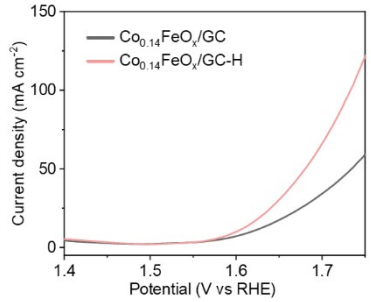

Figure S5. Polarization curves of $Co_{0.14}FeO_x$ loaded on a glassy carbon electrode (GC) with and without a constant magnetic field (3000 Oe).

Note: Under the external magnetic field, the catalytic activity of $Co_{0.14}FeO_x$/GC is significantly enhanced. This is consistent with experimental observations when carbon cloth is used as the substrate (Figure 3b). This demonstrates that carbon cloth substrate does not obviously affect the catalytic activity of the magnetically enhanced ferromagnetic $Co_{0.14}FeO_x$ material.

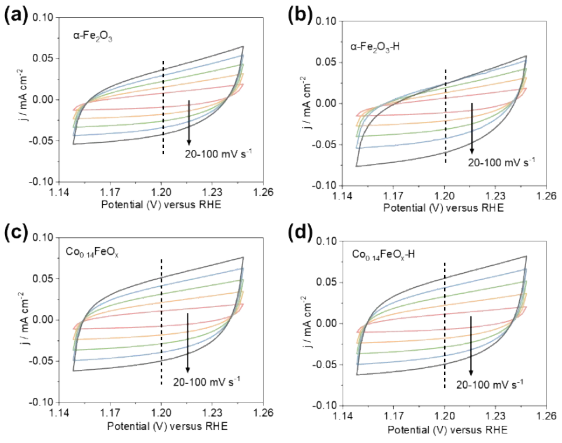

Figure S6. The CV curves of (a) α-Fe_2O_3, (b) α-Fe_2O_3 under the magnetic field, (c) $Co_{0.14}FeO_x$ and (d) $Co_{0.14}FeO_x$ under the magnetic field at scan rates with values in 20-100 mV s^{-1}.

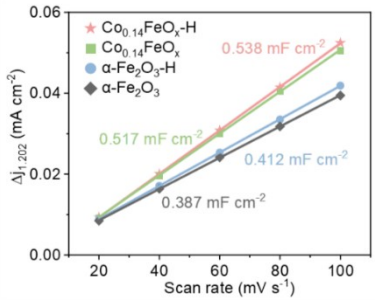

Figure S7. Double-layer capacitance (C_{dl}) plots of α-Fe_2O_3 and $Co_{0.14}FeO_x$ in different environments.

Note: $Co_{0.14}FeO_x$ possesses a C_{dl} of 0.517 mF cm^{-2}, which is slightly higher than the C_{dl} of α-Fe_2O_3. This finding indicates that $Co_{0.14}FeO_x$ has a larger ECSA, which may be due to the differences between the spinel structure and spherical particles. Furthermore, compared to the absence of an external field, the ECSA of both catalysts shows no significant change under the applied magnetic field. This suggests that the magnetic field has not had a noticeable effect on the number of active sites in the materials.

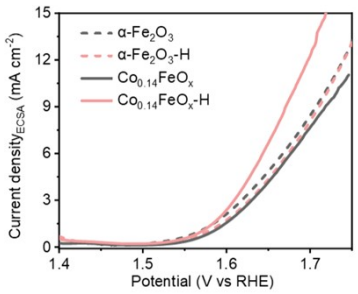

Figure S8. Polarization curves of Figure 3b normalized by ECSA.

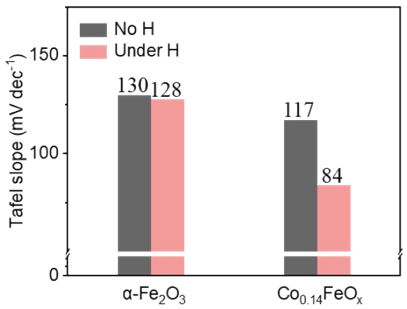

Figure S9. Bar diagram of the change in Tafel slopes for α-Fe_2O_3 and $Co_{0.14}FeO_x$ before and after applying an external magnetic field.

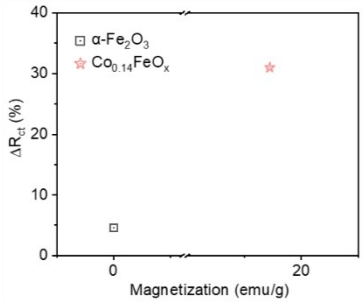

Figure S10. The relationship between the magnetization of α-Fe_2O_3 and $Co_{0.14}FeO_x$ under a 3000 Oe external magnetic field and the decrease in charge transfer resistance (ΔR_{ct} (%), Equation S2) after applying the magnetic field.

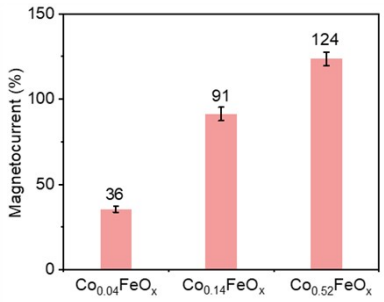

Figure S11. The average magnetocurrent in 1M KOH under the external magnetic field strength (3000 Oe) in the voltage range of 1.65 V to 1.75 V versus eversible hydrogen electrode for $Co_{0.04}FeO_x$, $Co_{0.14}FeO_x$ and $Co_{0.52}FeO_x$.

Note: As the cobalt content increases, the degree of enhancement in the material's OER activity under an external magnetic field becomes higher.

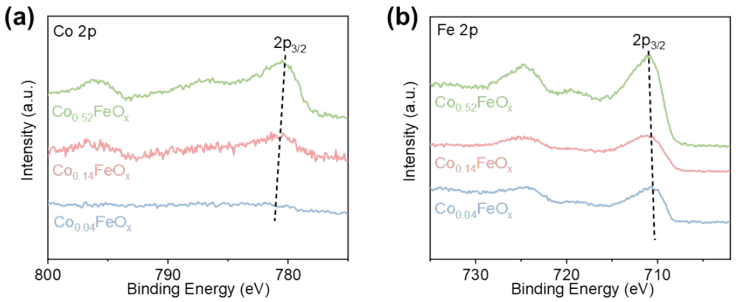

Figure S12. The (a) Co and (b) Fe 2p XPS spectra of samples with different Co contents

Note: With the increase in cobalt doping, the binding energy of the Co $2p_{3/2}$ orbital gradually decreases, while that of the Fe $2p_{3/2}$ orbital gradually increases. This indicates the presence of electronic interactions between Co and Fe atoms, and the charge transfer between Co and Fe is enhanced with the increase in cobalt doping.

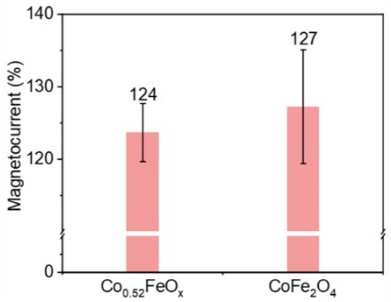

Figure S13. The average magnetocurrent in 1M KOH under the external magnetic field strength (3000 Oe) in the voltage range of 1.65 V to 1.75 V versus eversible hydrogen electrode for $Co_{0.52}FeO_x$ and $CoFe_2O_4$.

Note: Under the same magnetic field intensity, the catalytic performance enhancement of pure $CoFe_2O_4$ is slightly higher than that of $Co_{0.52}FeO_x$. This suggests that the electron transfer within $Co_{0.52}FeO_x$ does not appear to significantly enhance the spin polarization effect.

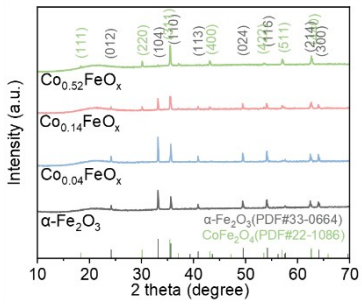

Figure S14. XRD patterns of samples with different Co contents.

Note: With the increase in cobalt content, the XRD diffraction peaks of the material gradually shift from α-Fe_2O_3 to $CoFe_2O_4$, indicating that cobalt doping induces a phase transition in the material.

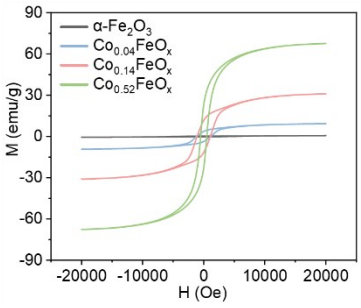

Figure S15. Magnetic hysteresis loops of samples with different Co contents.

Note: With the increase in cobalt doping, the saturation magnetization of the material increases. The above experimental result may be attributed to that as the cobalt doping level rises, the number of ordered magnetic domains under a constant external magnetic field increases,

leading to a more pronounced spin polarization effect, thereby enhancing the OER activity to a greater extent.

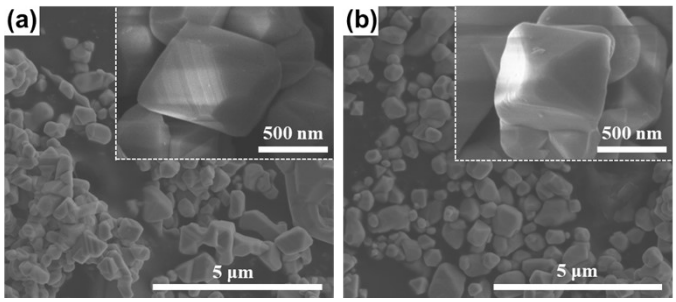

Figure S16. SEM images of $Co_{0.14}FeO_x$ after OER stability test (a) without and (b) with applying magnetic field.

Note: $Co_{0.14}FeO_x$ still retains a relatively intact spinel structure after the OER stability test both with and without applying a magnetic field.

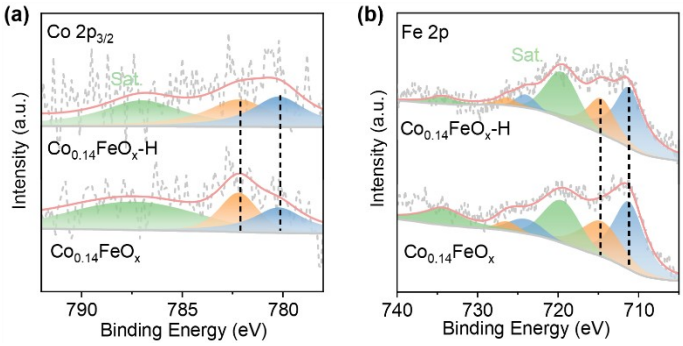

Figure S17. (a) Co $2p_{3/2}$ and (b) Fe 2p XPS spectra of $Co_{0.14}FeO_x$ after OER stability test with and without applying magnetic field.

Note: Compared to the absence of external magnetic field assistance, no distinct shifts in the characteristic Fe 2p and Co 2p peak positions were observed after the stability test of $Co_{0.14}FeO_x$ with magnetic field assistance.

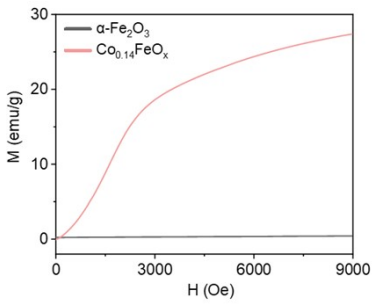

Figure S18. The initial magnetization curves of α-Fe_2O_3 and $Co_{0.14}FeO_x$ powders at room temperature (300 K).

Table S1. The mass fraction and molar atomic ratio of Co and Fe elements in α-Fe_2O_3 and $Co_{0.14}FeO_x$.

	Co (wt.%)	Fe (wt.%)	n_{Co} : n_{Fe}
α-Fe_2O_3	-	84.68	-
$Co_{0.14}FeO_x$	11.63	78.16	0.14

Table S2. The molar feed ratio and molar atomic ratio of Co and Fe elements.

	feed ratio (Co : Fe)	atomic ratio (Co : Fe)
$Co_{0.04}FeO_x$	1:2	0.04
$Co_{0.14}FeO_x$	2:1	0.14
$Co_{0.52}FeO_x$	8:1	0.52
$Co_{0.55}FeO_x$	12:1	0.55

References

(1) X. Sun, Q. Shao, Y. Pi, J. Guo and X. Huang, *J. Mater. Chem. A*, 2016, **4**, 51–58.